

FEDERATED ADVERSARIAL DOMAIN ADAPTATION

Xingchao Peng
 Boston University
 Boston, MA 02215, USA
 xpeng@bu.edu

Zijun Huang
 Columbia University
 New York City, NY 10027, USA
 zijun.huang@columbia.edu

Yizhe Zhu
 Rutgers University
 Piscataway, NJ 08854, USA
 yz530@scarletmail.rutgers.edu

Kate Saenko
 Boston University
 Boston, MA 02215, USA
 saenko@bu.edu

ABSTRACT

Federated learning improves data privacy and efficiency in machine learning performed over networks of distributed devices, such as mobile phones, IoT and wearable devices, etc. Yet models trained with federated learning can still fail to generalize to new devices due to the problem of domain shift. Domain shift occurs when the labeled data collected by source nodes statistically differs from the target node’s unlabeled data. In this work, we present a principled approach to the problem of federated domain adaptation, which aims to align the representations learned among the different nodes with the data distribution of the target node. Our approach extends adversarial adaptation techniques to the constraints of the federated setting. In addition, we devise a dynamic attention mechanism and leverage feature disentanglement to enhance knowledge transfer. Empirically, we perform extensive experiments on several image and text classification tasks and show promising results under unsupervised federated domain adaptation setting.

1 INTRODUCTION

Data generated by networks of mobile and IoT devices poses unique challenges for training machine learning models. Due to the growing storage/computational power of these devices and concerns about data privacy, it is increasingly attractive to keep data and computation locally on the device (Smith et al., 2017). *Federated Learning (FL)* (Mohassel & Rindal, 2018; Bonawitz et al., 2017; Mohassel & Zhang, 2017) provides a privacy-preserving mechanism to leverage such decentralized data and computation resources to train machine learning models. The main idea behind federated learning is to have each node learn on its own local data and not share either the data or the model parameters.

While federated learning promises better privacy and efficiency, existing methods ignore the fact that the data on each node are collected in a non-*i.i.d* manner, leading to *domain shift* between nodes (Quionero-Candela et al., 2009). For example, one device may take photos mostly indoors, while another mostly outdoors. In this paper, we address the problem of transferring knowledge from the decentralized nodes to a new node with a different data domain, without requiring any additional supervision from the user. We define this novel problem *Unsupervised Federated Domain Adaptation (UFDA)*, as illustrated in Figure 1(a).

There is a large body of existing work on unsupervised domain adaptation (Long et al., 2015; Ganin & Lempitsky, 2015; Tzeng et al., 2017; Zhu et al., 2017; Gong et al., 2012; Long et al., 2018), but the federated setting presents several additional challenges. First, the data are stored locally and cannot be shared, which hampers mainstream domain adaptation methods as they need to access both the

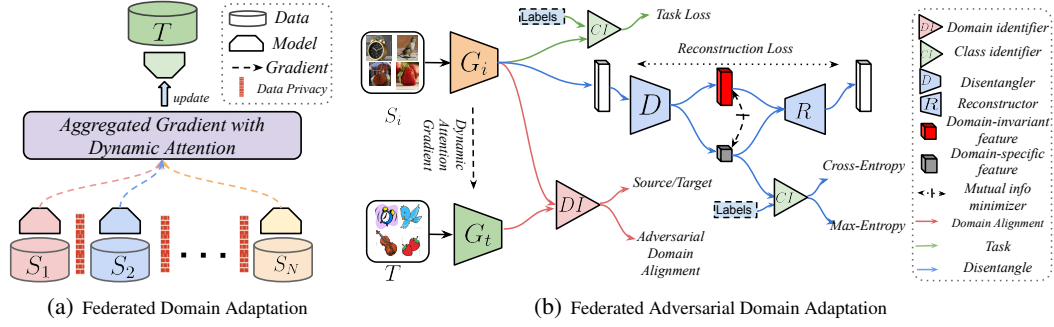


Figure 1: (a) We propose an approach for the UFDA setting, where data are not shareable between different domains. In our approach, models are trained separately on each source domain and their gradients are aggregated with *dynamic attention* mechanism to update the target model. (b) Our FADA model learns to extract *domain-invariant* features using adversarial domain alignment (red lines) and a feature *disentangler* (blue lines).

labeled source and unlabeled target data (Tzeng et al., 2014; Long et al., 2017; Ghifary et al., 2016; Sun & Saenko, 2016; Ganin & Lempitsky, 2015; Tzeng et al., 2017). Second, the model parameters are trained separately for each node and converge at different speeds, while also offering different contributions to the target node depending on how close the two domains are. Finally, the knowledge learned from source nodes is highly entangled (Bengio et al., 2013), which can possibly lead to *negative transfer* (Pan & Yang, 2010).

In this paper, we propose a solution to the above problems called *Federated Adversarial Domain Adaptation* (FADA) which aims to tackle domain shift in a federated learning system through adversarial techniques. Our approach preserves data privacy by training one model per source node and updating the target model with the aggregation of source gradients, but does so in a way that reduces domain shift. First, we analyze the federated domain adaptation problem from a theoretical perspective and provide a generalization bound. Inspired by our theoretical results, we propose an efficient adaptation algorithm based on adversarial adaptation and representation disentanglement applied to the federated setting. We also devise a *dynamic attention* model to cope with the varying convergence rates in the federated learning system. We conduct extensive experiments on real-world datasets, including image recognition and natural language tasks. Compared to baseline methods, we improve adaptation performance on all tasks, demonstrating the effectiveness of our devised model.

2 RELATED WORK

Unsupervised Domain Adaptation Unsupervised Domain Adaptation (UDA) aims to transfer the knowledge learned from a labeled source domain to an unlabeled target domain. Domain adaptation approaches proposed over the past decade include discrepancy-based methods (Tzeng et al., 2014; Long et al., 2017; Ghifary et al., 2014; Sun & Saenko, 2016; Peng & Saenko, 2018), reconstruction-based UDA models (Yi et al., 2017; Zhu et al., 2017; Hoffman et al., 2018; Kim et al., 2017), and adversary-based approaches (Liu & Tuzel, 2016; Tzeng et al., 2017; Liu et al., 2018a; Ganin & Lempitsky, 2015). For example, Ganin & Lempitsky (2015) propose a *gradient reversal* layer to perform adversarial training to a domain discriminator, inspired by the idea of adversarial learning. Tzeng et al. (2017) address unsupervised domain adaptation by adapting a deep CNN-based feature extractor/classifier across source and target domains via adversarial training. Ben-David et al. (2010) introduce an $\mathcal{H}\Delta\mathcal{H}$ -divergence to evaluate the domain shift and provide a generalization error bound for domain adaptation. These methods assume the data are centralized on one server, limiting their applicability to the distributed learning system.

Federated Learning Federated learning (Mohassel & Rindal, 2018; Rivest et al., 1978; Bonawitz et al., 2017; Mohassel & Zhang, 2017) is a decentralized learning approach which enables multiple clients to collaboratively learn a machine learning model while keeping the training data and model parameters on local devices. Inspired by Homomorphic Encryption (Rivest et al., 1978), (Gilad-Bachrach et al., 2016) propose CryptoNets to enhance the efficiency of data encryption, achieving higher federated learning performance. Bonawitz et al. (2017) introduce a secure aggregation scheme

to update the machine learning models under their federated learning framework. Recently, Mohassel & Zhang (2017) propose SecureML to support privacy-preserving collaborative training in a multi-client federated learning system. However, these methods mainly aim to learn a single global model across the data and have no convergence guarantee, which limits their ability to deal with non-*i.i.d.* data. To address the non-*i.i.d.* data, Smith et al. (2017) introduce federated multi-task learning, which learns a separate model for each node. Liu et al. (2018b) propose semi-supervised federated transfer learning in a privacy-preserving setting. However, their models involve full or semi-supervision. The work proposed here is, to our best knowledge, the first federated learning framework to consider unsupervised domain adaptation.

Feature Disentanglement Deep neural networks are known to extract features where multiple hidden factors are highly entangled. Learning disentangled representations can help remove irrelevant and domain-specific features and model only the relevant factors of data variation. To this end, recent work (Mathieu et al., 2016; Makhzani et al., 2016; Liu et al., 2018a; Odena et al., 2017) explores the learning of interpretable representations using generative adversarial networks (GANs) (Goodfellow et al., 2014) and variational autoencoders (VAEs) (Kingma & Welling, 2013). Under the fully supervised setting, (Odena et al., 2017) propose an auxiliary classifier GAN (AC-GAN) to achieve representation disentanglement. (Liu et al., 2018a) introduce a unified feature disentanglement framework to learn domain-invariant features from data across different domains. (Kingma et al., 2014) also extend VAEs into the semi-supervised setting for representation disentanglement. (Lee et al., 2018) propose to disentangle the features into a domain-invariant content space and a domain-specific attributes space, producing diverse outputs without paired training data. Inspired by these works, we propose a method to disentangle the *domain-invariant* features from *domain-specific* features, using an adversarial training process. In addition, we propose to minimize the mutual information between the *domain-invariant* features and *domain-specific* features to enhance the feature disentanglement.

3 GENERALIZATION BOUND FOR FEDERATED DOMAIN ADAPTATION

We first define the notation and review a typical theoretical error bound for single-source domain adaptation (Ben-David et al., 2007; Blitzer et al., 2008) devised by Ben-David *et al.* Then we describe our derived error bound for unsupervised federated domain adaptation. We mainly focus on the high-level interpretation of the error bound here and refer our readers to the appendix (see supplementary material) for proof details.

Notation. Let \mathcal{D}_S^1 and \mathcal{D}_T denote source and target distribution on input space \mathcal{X} and a ground-truth labeling function $g : \mathcal{X} \rightarrow \{0, 1\}$. A *hypothesis* is a function $h : \mathcal{X} \rightarrow \{0, 1\}$ with the *error* w.r.t the ground-truth labeling function g : $\epsilon_S(h, g) := \mathbb{E}_{\mathbf{x} \sim \mathcal{D}_S} [|h(\mathbf{x}) - g(\mathbf{x})|]$. We denote the risk and empirical risk of hypothesis h on \mathcal{D}_S as $\epsilon_S(h)$ and $\hat{\epsilon}_S(h)$. Similarly, the risk and empirical risk of h on \mathcal{D}_T are denoted as $\epsilon_T(h)$ and $\hat{\epsilon}_T(h)$. The \mathcal{H} -divergence between two distributions \mathcal{D} and \mathcal{D}' is defined as: $d_{\mathcal{H}}(\mathcal{D}, \mathcal{D}') := 2 \sup_{A \in \mathcal{A}_{\mathcal{H}}} |\Pr_{\mathcal{D}}(A) - \Pr_{\mathcal{D}'}(A)|$, where \mathcal{H} is a hypothesis class for input space \mathcal{X} , and $\mathcal{A}_{\mathcal{H}}$ denotes the collection of subsets of \mathcal{X} that are the support of some hypothesis in \mathcal{H} .

The $\mathcal{H}\Delta\mathcal{H}$ divergence of a measurable hypothesis class \mathcal{H} is defined as: $\mathcal{H}\Delta\mathcal{H} := \{h(\mathbf{x}) \oplus h'(\mathbf{x}) | h, h' \in \mathcal{H}\}$, (\oplus : the XOR operation). We denote the optimal hypothesis that achieves the minimum risk on the source and the target as $h^* := \arg \min_{h \in \mathcal{H}} \epsilon_S(h) + \epsilon_T(h)$ and the error of h^* as $\lambda := \epsilon_S(h^*) + \epsilon_T(h^*)$. Blitzer et al. (2007b) prove the following error bound on the target domain.

Theorem 1. Let \mathcal{H} be a hypothesis space of VC-dimension d and $\hat{\mathcal{D}}_S, \hat{\mathcal{D}}_T$ be the empirical distribution induced by samples of size m drawn from \mathcal{D}_S and \mathcal{D}_T . Then with probability at least $1 - \delta$ over the choice of samples, for each $h \in \mathcal{H}$,

$$\epsilon_T(h) \leq \hat{\epsilon}_S(h) + \frac{1}{2} \hat{d}_{\mathcal{H}\Delta\mathcal{H}}(\hat{\mathcal{D}}_S, \hat{\mathcal{D}}_T) + 4 \sqrt{\frac{2d \log(2m) + \log(4/\delta)}{m}} + \lambda \quad (1)$$

Let $\mathcal{D}_S = \{\mathcal{D}_{S_i}\}_{i=1}^N$, and $\mathcal{D}_T = \{\mathcal{D}_j^t\}_{j=1}^{n_t}$ be N source domains and the target domain in a UFDA system, where $\mathcal{D}_{S_i} = \{(\mathbf{x}_j^s, \mathbf{y}_j^s)\}_{j=1}^{n_i}$. In federated domain adaptation system, \mathcal{D}_S is distributed on

¹In this literature, the calligraphic \mathcal{D} denotes data distribution, and italic D denotes domain discriminator.

N nodes and the data are not shareable with each other in the training process. The classical domain adaptation algorithms aim to minimize the target risk $\epsilon_T(h) := \Pr_{(\mathbf{x}, y) \sim \mathcal{D}_T} [h(\mathbf{x}) \neq y]$. However, in a UFDA system, one model cannot directly get access to data stored on different nodes for security and privacy reasons. To address this issue, we propose to learn separate models for each distributed source domain $h_S = \{h_{S_i}\}_{i=1}^N$. The target hypothesis h_T is the aggregation of the parameters of h_S , i.e. $h_T := \sum_{i=1}^N \alpha_i h_{S_i}$, $\forall \alpha \in \mathbb{R}_+^N$, $\sum_{i \in [N]} \alpha_i = 1$. We can then derive the following error bound:

Theorem 2. (Weighted error bound for federated domain adaptation). *Let \mathcal{H} be a hypothesis class with VC-dimension d and $\{\widehat{\mathcal{D}}_{S_i}\}_{i=1}^N$, $\widehat{\mathcal{D}}_T$ be empirical distributions induced by a sample of size m from each source domain and target domain in a federated learning system, respectively. Then, $\forall \alpha \in \mathbb{R}_+^N$, $\sum_{i=1}^N \alpha_i = 1$, with probability at least $1 - \delta$ over the choice of samples, for each $h \in \mathcal{H}$,*

$$\epsilon_T(h_T) \leq \underbrace{\widehat{\epsilon}_{\tilde{S}}\left(\sum_{i \in [N]} \alpha_i h_{S_i}\right)}_{\text{error on source}} + \sum_{i \in [N]} \alpha_i \underbrace{\left(\frac{1}{2} \widehat{d}_{\mathcal{H}\Delta\mathcal{H}}(\widehat{\mathcal{D}}_{S_i}, \widehat{\mathcal{D}}_T) + \lambda_i\right)}_{(\mathcal{D}_{S_i}, \mathcal{D}_T) \text{ divergence}} + 4 \underbrace{\sqrt{\frac{2d \log(2Nm) + \log(4/\delta)}{Nm}}}_{\text{VC-Dimension Constraint}} \quad (2)$$

where λ_i is the risk of the optimal hypothesis on the mixture of \mathcal{D}_{S_i} and T , and \tilde{S} is the mixture of source samples with size Nm . $\widehat{d}_{\mathcal{H}\Delta\mathcal{H}}(\widehat{\mathcal{D}}_{S_i}, \widehat{\mathcal{D}}_T)$ denotes the divergence between domain S_i and T .

Comparison with Existing Bounds The bound in (2) is extended from (1) and they are equivalent if only one source domain exists ($N = 1$). Mansour et al. (2009) provide a generalization bound for multiple-source domain adaptation, assuming that the target domain is a mixture of the N source domains. In contrast, in our error bound (2), the target domain is assumed to be a novel domain, resulting in a bound involving $\mathcal{H}\Delta\mathcal{H}$ discrepancy (Ben-David et al., 2010) and the VC-dimensional constraint (Vapnik & Vapnik, 1998). Blitzer et al. (2007b) propose a generalization bound for semi-supervised multi-source domain adaptation, assuming that partial target labels are available. Our generalization bound is devised for unsupervised learning. Zhao et al. (2018) introduce classification and regression error bounds for multi-source domain adaptation. However, these error bounds assume that the multiple source and target domains exactly share the same hypothesis. In contrast, our error bound involves multiple hypotheses.

4 FEDERATED ADVERSARIAL DOMAIN ADAPTATION

The error bound in Theorem (2) demonstrates the importance of the weight α and the discrepancy $d_{\mathcal{H}\Delta\mathcal{H}}(\mathcal{D}_S, \mathcal{D}_T)$ in unsupervised federated domain adaptation. Inspired by this, we propose dynamic attention model to learn the weight α and federated adversarial alignment to minimize the discrepancy between the source and target domains, as shown in Figure 1. In addition, we leverage representation disentanglement to extract *domain-invariant* representations to further enhance knowledge transfer.

Dynamic Attention In a federated domain adaptation system, the models on different nodes have different convergence rates. In addition, the domain shifts between the source domains and target domain are different, leading to a phenomenon where some nodes may have no contribution or even *negative transfer* (Pan & Yang, 2010) to the target domain. To address this issue, we propose dynamic attention, which is a mask on the gradients from source domains. The philosophy behind the dynamic attention is to increase the weight of those nodes whose gradients are beneficial to the target domain and limit the weight of those whose gradients are detrimental to the target domain. Specifically, we leverage the *gap statistics* (Tibshirani et al., 2001) to evaluate how well the target features f^t can be clustered with unsupervised clustering algorithms (K-Means). Assuming we have k clusters, the *gap statistics* are computed as:

$$I = \sum_{r=1}^k \frac{1}{2n_r} \sum_{i,j \in C_r} \|f_i^t - f_j^t\|_2 \quad (3)$$

where we have clusters C_1, C_2, \dots, C_k , with C_r denoting the indices of observations in cluster r , and $n_r = |C_r|$. Intuitively, a smaller *gap statistics* value indicates the feature distribution has smaller intra-class variance. We measure the contribution of each source domain by the *gap statistics gain* between two consecutive iterations: $I_i^{\text{gain}} = I_i^{p-1} - I_i^p$ (p indicating training step), denoting how much the clusters can be improved before and after the target model is updated with the i -th source model's gradient. The mask on the gradients from source domains is defined as $\text{Softmax}(I_1^{\text{gain}}, I_2^{\text{gain}}, \dots, I_N^{\text{gain}})$.

Algorithm 1 Federated Adversarial Domain Adaptation

Input: N source domains $\mathcal{D}_S = \{\mathcal{D}_{S_i}\}_{i=1}^N$; a target domain $\mathcal{D}_t = \{\mathcal{X}_j^t\}_{j=1}^{n_t}$; N models trained on source domain $\{\Theta^1, \Theta^2, \dots, \Theta^N\}$; target model Θ^T , disentangler D , domain identifier DI , mutual information estimator M

Output: well-trained $\hat{\Theta}^T$.

Model Initialization .

```

1: while not converged do
2:   for  $k$  do 1:N
3:     Sample mini-batch from  $\{(\mathbf{x}_i^s, y_i^s)\}_{i=1}^{n_s}$  and  $\{\mathbf{x}_j^t\}_{j=1}^{n_t}$ ;
4:     Compute gradient with cross-entropy classification loss, update  $\Theta^k$ .
5:     Domain Alignment:
6:     Update  $\{\Theta^k, \Theta^T\}$  with Eq. 4 and Eq. 5 to align the domain distribution;
7:     Domain Disentangle:
8:     update  $DI$  with Eq. 6
9:     update  $D$  and  $\{\Theta^k\}$  with Eq. 7
10:    Mutual Information Minimization:
11:    Calculate mutual information between the disentangled feature pair  $(f_{di}, f_{ds})$  with  $M$ 
12:    Update  $D, M$  by Eq.8;
13:  end for
14:  Dynamic weight:
15:  Calculate dynamic weight by Eq. 3
16:  Update  $\Theta^T$  by aggregated  $\{\Theta^1, \Theta^2, \dots, \Theta^N\}$  with the computed dynamic weight;
17: end while
18: return  $\hat{\Theta}^1 = \Theta^1; \hat{\Theta}^2 = \Theta^2; \dots; \hat{\Theta}^N = \Theta^N; \hat{\Theta}^T = \Theta^T$ .
    
```

Federated Adversarial Alignment The performance of machine learning models degrades rapidly with the presence of domain discrepancy (Long et al., 2015). To address this issue, existing work (Hoffman et al., 2018; Tzeng et al., 2015) proposes to minimize the discrepancy with an adversarial training process. For example, Tzeng et al. (2015) proposes the domain confusion objective, under which the feature extractor is trained with a cross-entropy loss against a uniform distribution. However, these models require access to the source and target data simultaneously, which is prohibitive in UFDA. In the federated setting, we have multiple source domains and the data are locally stored in a privacy-preserving manner, which means we cannot train a single model which has access to the source domain and target domain simultaneously. To address this issue, we propose federated adversarial alignment that divides optimization into two independent steps, a domain-specific local feature extractor and a global discriminator. Specifically, (1) for each domain, we train a local feature extractor, G_i for \mathcal{D}_i and G_t for \mathcal{D}_t , (2) for each $(\mathcal{D}_i, \mathcal{D}_t)$ source-target domain pair, we train an adversarial domain classifier D to align the distributions. Note that D only gets access to the output vectors of G_i and G_t , without violating the UFDA setting. Given the i -th source domain data \mathbf{X}^{S_i} , target data \mathbf{X}^T , the objective for D are defined as follows:

$$\mathcal{L}_{adv_D}(\mathbf{X}^{S_i}, \mathbf{X}^T, G_i, G_t) = -\mathbb{E}_{\mathbf{x}^{S_i} \sim \mathbf{X}^{S_i}} [\log D(G_i(\mathbf{x}^{S_i}))] - \mathbb{E}_{\mathbf{x}^t \sim \mathbf{X}^t} [\log(1 - D(G_t(\mathbf{x}^t)))] \quad (4)$$

In the second step, \mathcal{L}_{adv_D} remains unchanged, but \mathcal{L}_{adv_G} is updated with the following objective:

$$\mathcal{L}_{adv_G}(\mathbf{X}^{S_i}, \mathbf{X}^T, D) = -\mathbb{E}_{\mathbf{x}^{S_i} \sim \mathbf{X}^{S_i}} [\log D(G_i(\mathbf{x}^{S_i}))] - \mathbb{E}_{\mathbf{x}^t \sim \mathbf{X}^t} [\log D(G_t(\mathbf{x}^t))] \quad (5)$$

Representation Disentanglement We employ *adversarial disentanglement* to extract the *domain-invariant* features. Specifically, we first train the disentangler and the K -way class identifier C to correctly predict the labels with a cross-entropy loss, based on f_{di} and f_{ds} features. The objective is:

$$\mathcal{L}_{ce} = -\mathbb{E}_{(\mathbf{x}^{S_i}, \mathbf{y}^{S_i}) \sim \hat{\mathcal{D}}_{S_i}} \sum_{k=1}^K \mathbb{1}[k = \mathbf{y}^{S_i}] \log(C_s(f_{di})) - \mathbb{E}_{(\mathbf{x}^{S_i}, \mathbf{y}^{S_i}) \sim \hat{\mathcal{D}}_{S_i}} \sum_{k=1}^K \mathbb{1}[k = \mathbf{y}^{S_i}] \log(C_s(f_{ds})) \quad (6)$$

where f_{di}, f_{ds} denote the *domain-invariant* and *domain-specific* features respectively. In the next step, we freeze the class identifier and only train the feature disentangler to confuse the class identifier C by generating the *domain-specific* features f_{ds} , as shown in Figure 1. This can be achieved by minimizing the negative entropy loss of the predicted class distribution. The objective is as follows:

$$\mathcal{L}_{ent} = -\frac{1}{n_{S_i}} \sum_{j=1}^{n_{S_i}} \log C(f_{ds}^j) \quad (7)$$

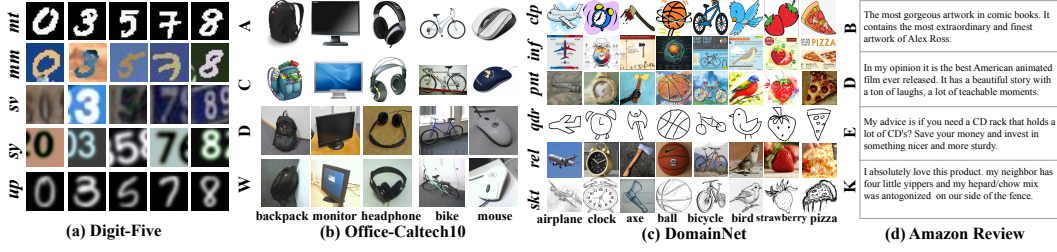


Figure 2: We demonstrate the effectiveness of FADA on four datasets: (1) “Digit-Five”, which includes MNIST (*mt*), MNIST-M (*mm*), SVHN (*sv*), Synthetic (*syn*), and USPS (*up*). (2) Office-Caltech10 dataset, which contains *Amazon* (A), *Caltech* (C), *DSLR* (D), and *Webcam* (W). (3) DomainNet dataset, which includes: *clipart* (*clp*), *infograph* (*inf*), *painting* (*pnt*), *quickdraw* (*qdr*), *real* (*rel*), and *sktech* (*skt*). (4) Amazon Review dataset, which contains review for *Books* (B), *DVDs* (D), *Electronics* (E), and *Kitchen & housewares* (K).

To enhance the disentanglement, we minimize the mutual information between *domain-invariant* features and *domain-specific* features, following Peng et al. (2019). Specifically, the mutual information is defined as $I(f_{di}; f_{ds}) = \int_{\mathcal{P} \times \mathcal{Q}} \log \frac{d\mathbb{P}_{\mathcal{P}\mathcal{Q}}}{d\mathbb{P}_{\mathcal{P}} \otimes \mathbb{P}_{\mathcal{Q}}} d\mathbb{P}_{\mathcal{P}\mathcal{Q}}$, where $\mathbb{P}_{\mathcal{P}\mathcal{Q}}$ is the joint probability distribution of (f_{di}, f_{ds}) , and $\mathbb{P}_{\mathcal{P}} = \int_{\mathcal{Q}} d\mathbb{P}_{\mathcal{P}\mathcal{Q}}$, $\mathbb{P}_{\mathcal{Q}} = \int_{\mathcal{P}} d\mathbb{P}_{\mathcal{P}\mathcal{Q}}$ are the marginals. Despite being a pivotal measure across different distributions, the mutual information is only tractable for discrete variables, for a limited family of problems where the probability distributions are unknown (Belghazi et al., 2018). Following Peng et al. (2019), we adopt the Mutual Information Neural Estimator (MINE) (Belghazi et al., 2018) to estimate the mutual information by leveraging a neural network T_{θ} : $\widehat{I(\mathcal{P}; \mathcal{Q})}_n = \sup_{\theta \in \Theta} \mathbb{E}_{\mathbb{P}_{\mathcal{P}\mathcal{Q}}^{(n)}} [T_{\theta}] - \log(\mathbb{E}_{\mathbb{P}_{\mathcal{P}}^{(n)} \otimes \mathbb{P}_{\mathcal{Q}}^{(n)}} [e^{T_{\theta}}])$. Practically, MINE can be calculated as $I(\mathcal{P}; \mathcal{Q}) = \int \int \mathbb{P}_{\mathcal{P}\mathcal{Q}}^n(p, q) T(p, q, \theta) - \log(\int \mathbb{P}_{\mathcal{P}}^n(p) \mathbb{P}_{\mathcal{Q}}^n(q) e^{T(p, q, \theta)})$. To avoid computing the integrals, we leverage Monte-Carlo integration to calculate the estimation:

$$I(\mathcal{P}, \mathcal{Q}) = \frac{1}{n} \sum_{i=1}^n T(p, q, \theta) - \log\left(\frac{1}{n} \sum_{i=1}^n e^{T(p, q', \theta)}\right) \quad (8)$$

where (p, q) are sampled from the joint distribution and q' is sampled from the marginal distribution. The *domain-invariant* and *domain-specific* features are forwarded to a reconstructor with a L2 loss to reconstruct the original features, aiming to keep the representation integrity, as shown in Figure 1(b).

Optimization Our model is trained in an end-to-end fashion. We train federated alignment and representation disentanglement component with Stochastic Gradient Descent (Kiefer et al., 1952). The federated adversarial alignment loss and representation disentanglement loss are optimized together with the task loss. The detailed training procedure is presented in Algorithm 1.

5 EXPERIMENTS

We test our model on the following tasks: digit classification (*Digit-Five*), object recognition (*Office-Caltech10* (Gong et al., 2012), *DomainNet* (Peng et al., 2018)) and sentiment analysis (*Amazon Review* dataset (Blitzer et al., 2007a)). Figure 2 shows some data samples and Table 8 (see supplementary material) shows the number of data per domain we used in our experiments. We perform our experiments on a 10 Titan-Xp GPU cluster and simulate the federated system on a single machine (as the data communication is not the main focus of this paper). Our model is implemented with PyTorch. We repeat every experiment 10 times on the *Digit-Five* and *Amazon Review* datasets, and 5 times on the *Office-Caltech10* and *DomainNet* (Peng et al., 2018) datasets, reporting the mean and standard derivation of accuracy. To better explore the effectiveness of different components of our model, we propose three different ablations, *i.e.* model **I**: with *dynamic attention*; model **II**: **I** + *adversarial alignment*; and model **III**: **II** + *representation disentanglement*.

| Models | <i>mt,sv,sy,up</i> → <i>mm</i> | <i>mm,sv,sy,up</i> → <i>mt</i> | <i>mt,mm,sy,up</i> → <i>sv</i> | <i>mt,mm,sv,up</i> → <i>sy</i> | <i>mt,mm,sv,sy</i> → <i>up</i> | Avg |
|-------------------------------|--------------------------------|--------------------------------|--------------------------------|--------------------------------|--------------------------------|-------------|
| Source Only | 63.3±0.7 | 90.5±0.8 | 88.7±0.8 | 63.5±0.9 | 82.4±0.6 | 77.7 |
| DAN | 63.7±0.7 | 96.3±0.5 | 94.2±0.8 | 62.4±0.7 | 85.4±0.7 | 80.4 |
| DANN | 71.3±0.5 | 97.6±0.7 | 92.3±0.8 | 63.4±0.7 | 85.3±0.8 | 82.1 |
| Source Only | 49.6±0.8 | 75.4±1.3 | 22.7±0.9 | 44.3±0.7 | 75.5±1.4 | 53.5 |
| AdaBN | 59.3±0.8 | 75.3±0.7 | 34.2±0.6 | 59.7±0.7 | 87.1±0.9 | 61.3 |
| AutoDIAL | 60.7±1.6 | 76.8±0.9 | 32.4±0.5 | 58.7±1.2 | 90.3±0.9 | 65.8 |
| <i>f</i> -DANN | 59.5±0.6 | 86.1±1.1 | 44.3±0.6 | 53.4±0.9 | 89.7±0.9 | 66.6 |
| <i>f</i> -DAN | 57.5±0.8 | 86.4±0.7 | 45.3±0.7 | 58.4±0.7 | 90.8±1.1 | 67.7 |
| FADA+attention (I) | 44.2±0.7 | 90.5±0.8 | 27.8±0.5 | 55.6±0.8 | 88.3±1.2 | 61.3 |
| FADA+adversarial (II) | 58.2±0.8 | 92.5±0.9 | 48.3±0.6 | 62.1±0.5 | 90.6±1.1 | 70.3 |
| FADA+disentangle (III) | 62.5±0.7 | 91.4±0.7 | 50.5±0.3 | 71.8±0.5 | 91.7±1.0 | 73.6 |

Table 1: Accuracy (%) on “Digit-Five” dataset with UFDA protocol. FADA achieves **73.6%**, outperforming other baselines. We incrementally add each component to our model, aiming to study their effectiveness on the final results. (model **I**: with *dynamic attention*; model **II**: **I**+*adversarial alignment*; model **III**: **II**+*representation disentanglement*. *mt*, *up*, *sv*, *sy*, *mm* are abbreviations for *MNIST*, *USPS*, *SVHN*, *Synthetic Digits*, *MNIST-M*.)

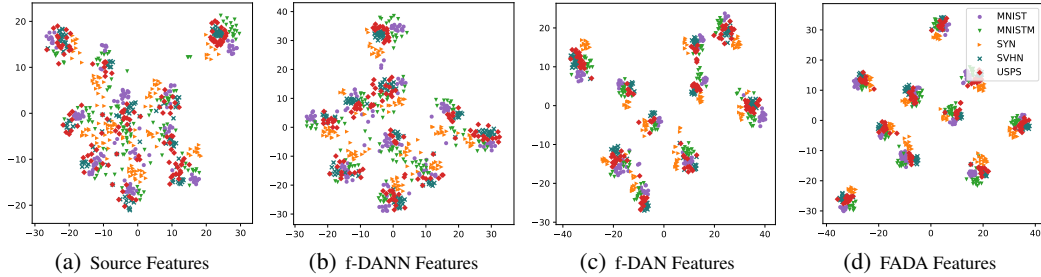


Figure 3: Feature visualization: t-SNE plot of source-only features, f-DANN (Ganin & Lempitsky, 2015) features, f-DAN (Long et al., 2015) features and FADA features in *sv,mm,mt,sy*→*up* setting. We use different markers and colors to denote different domains. The data points from target domain have been denoted by red for better visual effect. (Best viewed in color.)

5.1 EXPERIMENTS ON DIGIT RECOGNITION

Digit-Five This dataset is a collection of five benchmarks for digit recognition, namely *MNIST* (LeCun et al., 1998), *Synthetic Digits* (Ganin & Lempitsky, 2015), *MNIST-M* (Ganin & Lempitsky, 2015), *SVHN*, and *USPS*. In our experiments, we take turns setting one domain as the target domain and the rest as the distributed source domains, leading to five transfer tasks. The detailed architecture of our model can be found in Table 6 (see supplementary material).

Since many DA models (Saito et al., 2018; French et al., 2018; Hoffman et al., 2018) require access to data from different domains, it is infeasible to directly compare our model to these baselines. Instead, we compare our model to the following popular domain adaptation baselines: Domain Adversarial Neural Network (**DANN**) (Ganin & Lempitsky, 2015), Deep Adaptation Network (**DAN**) (Long et al., 2015), Automatic Domain Alignment Layers (**AutoDIAL**) (Carlucci et al., 2017), and Adaptive Batch Normalization (**AdaBN**) Li et al. (2016). Specifically, DANN minimizes the domain gap between source domain and target domain with a *gradient reversal* layer. DAN applies multi-kernel MMD loss (Gretton et al., 2007) to align the source domain with the target domain in Reproducing Kernel Hilbert Space. AutoDIAL introduces domain alignment layer to deep models to match the source and target feature distributions to a reference one. AdaBN applies Batch Normalization layer (Ioffe & Szegedy, 2015) to facilitate the knowledge transfer between the source and target domains. When conducting the baseline experiments, we use the code provided by the authors and modify the original settings to fit federated DA setting (*i.e.* each domain has its own model), denoted by *f*-DAN and *f*-DANN. In addition, to demonstrate the difficulty of UFDA where accessing all source data with a single model is prohibitive, we also perform the corresponding *multi-source DA* experiments (shared source data).

| Method | C,D,W \rightarrow A | A,D,W \rightarrow C | A,C,W \rightarrow D | A,C,D \rightarrow W | Average |
|-------------------------------|--------------------------------|--------------------------------|--------------------------------|--------------------------------|-------------|
| AlexNet | 80.1 \pm 0.4 | 86.9 \pm 0.3 | 82.7 \pm 0.5 | 85.1 \pm 0.3 | 83.7 |
| <i>f</i> -DAN | 82.5 \pm 0.5 | 87.2 \pm 0.4 | 85.6 \pm 0.4 | 86.1 \pm 0.3 | 85.4 |
| <i>f</i> -DANN | 83.1 \pm 0.4 | 86.5 \pm 0.5 | 84.8 \pm 0.5 | 86.4 \pm 0.5 | 85.2 |
| FADA+attention (I) | 81.2 \pm 0.3 | 87.1 \pm 0.6 | 83.5 \pm 0.5 | 85.9 \pm 0.4 | 84.4 |
| FADA+adversarial (II) | 83.1 \pm 0.6 | 87.8 \pm 0.4 | 85.4 \pm 0.4 | 86.8 \pm 0.5 | 85.8 |
| FADA+disentangle (III) | 84.3\pm0.6 | 88.4 \pm 0.5 | 86.1 \pm 0.4 | 87.3 \pm 0.5 | 86.5 |
| ResNet101 | 81.9 \pm 0.5 | 87.9 \pm 0.3 | 85.7 \pm 0.5 | 86.9 \pm 0.4 | 85.6 |
| AdaBN | 82.2 \pm 0.4 | 88.2 \pm 0.6 | 85.9 \pm 0.7 | 87.4 \pm 0.8 | 85.7 |
| AutoDIAL | 83.3 \pm 0.6 | 87.7 \pm 0.8 | 85.6 \pm 0.7 | 87.1 \pm 0.6 | 85.9 |
| <i>f</i> -DAN | 82.7 \pm 0.3 | 88.1 \pm 0.5 | 86.5 \pm 0.3 | 86.5 \pm 0.3 | 85.9 |
| <i>f</i> -DANN | 83.5 \pm 0.4 | 88.5 \pm 0.3 | 85.9 \pm 0.5 | 87.1 \pm 0.4 | 86.3 |
| FADA+attention (I) | 82.1 \pm 0.5 | 87.5 \pm 0.3 | 85.8 \pm 0.4 | 87.3 \pm 0.5 | 85.7 |
| FADA+adversarial (II) | 83.2 \pm 0.4 | 88.4 \pm 0.3 | 86.4 \pm 0.5 | 87.8 \pm 0.4 | 86.5 |
| FADA+disentangle (III) | 84.2 \pm 0.5 | 88.7\pm0.5 | 87.1\pm0.6 | 88.1\pm0.4 | 87.1 |

Table 2: Accuracy on *Office-Caltech10* dataset with unsupervised federated domain adaptation protocol. The upper table shows the results for AlexNet backbone and the table below shows the results for ResNet backbone.

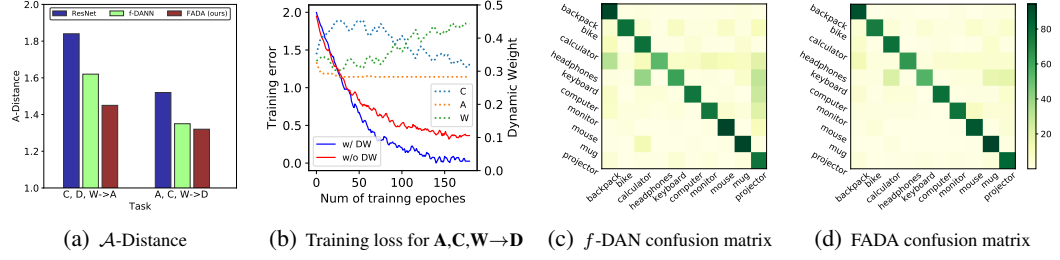


Figure 4: (a) A-Distance of ResNet, *f*-DANN, and FADA features on two different tasks. (b) training errors and dynamic weight on A,C,W \rightarrow D task. (c)-(d) confusion matrices of *f*-DAN, and FADA on A,C,D \rightarrow W task.

Results and Analysis The experimental results are shown in Table 1. From the results, we can make the following observations. (1) Model III achieves 73.6% average accuracy, significantly outperforming the baselines. (2) The results of model I and model II demonstrate the effectiveness of *dynamic attention* and *adversarial alignment*. (3) Federated DA displays much weaker results than *multi-source DA*, demonstrating that the newly proposed UFDA learning setting is very challenging.

To dive deeper into the feature representation of our model versus other baselines, we plot in Figure 3(a)-3(d) the t-SNE embeddings of the feature representations learned on *mm,mt,sv,sy* \rightarrow *up* task with source-only features, *f*-DANN features, *f*-DAN features and FADA features, respectively. We observe that the feature embeddings of our model have smaller intra-class variance and larger inter-class variance than *f*-DANN and *f*-DAN, demonstrating that our model is capable of generating the desired feature embedding and can extract *domain-invariant* features across different domains.

5.2 EXPERIMENTS ON OFFICE-CALTECH10

Office-Caltech10 (Gong et al., 2012) This dataset contains 10 common categories shared by Office-31 (Saenko et al., 2010) and Caltech-256 datasets (Griffin et al., 2007). It contains four domains: *Caltech* (C), which are sampled from Caltech-256 dataset, *Amazon* (A), which contains images collected from *amazon.com*, *Webcam* (W) and *DSLR* (D), which contains images taken by web camera and DSLR camera under office environment.

We leverage two popular networks as the backbone of feature generator *G*, *i.e.* AlexNet (Krizhevsky et al., 2012) and ResNet (He et al., 2016). Both the networks are pre-trained on ImageNet (Deng et al., 2009). Other components of our model are randomly initialized with the normal distribution. In the learning process, we set the learning rate of randomly initialized parameters to ten times of

| Models | <i>inf,pnt,qdr, rel,skt→clp</i> | <i>clp,pnt,qdr, rel,skt→inf</i> | <i>clp,inf,qdr, rel,skt→pnt</i> | <i>clp,inf,pnt, rel,skt→qdr</i> | <i>clp,inf,pnt, qdr,skt→rel</i> | <i>clp,inf,pnt, qdr,rel→skt</i> | Avg |
|-------------------------------|-------------------------------------|-------------------------------------|-------------------------------------|-------------------------------------|-------------------------------------|-------------------------------------|-------------|
| AlexNet | 39.2±0.7 | 12.7±0.4 | 32.7±0.4 | 5.9±0.7 | 40.3±0.5 | 22.7±0.6 | 25.6 |
| <i>f</i> -DAN | 41.6±0.6 | 13.7±0.5 | 36.3±0.5 | 6.5±0.5 | 43.5±0.8 | 22.9±0.5 | 27.4 |
| <i>f</i> -DANN | 42.6±0.8 | 14.1±0.7 | 35.2±0.3 | 6.2±0.7 | 42.9±0.5 | 22.7±0.7 | 27.2 |
| FADA+disentangle (III) | 44.9±0.7 | 15.9±0.6 | 36.3±0.8 | 8.6±0.8 | 44.5±0.6 | 23.2±0.8 | 28.9 |
| ResNet101 | 41.6±0.6 | 14.5±0.7 | 35.7±0.7 | 8.4±0.7 | 43.5±0.7 | 23.3±0.7 | 27.7 |
| <i>f</i> -DAN | 43.5±0.7 | 14.1±0.6 | 37.6±0.7 | 8.3±0.6 | 44.5±0.5 | 25.1±0.5 | 28.9 |
| <i>f</i> -DANN | 43.1±0.8 | 15.2±0.9 | 35.7±0.4 | 8.2±0.6 | 45.2±0.7 | 27.1±0.6 | 29.1 |
| FADA+disentangle (III) | 45.3±0.7 | 16.3±0.8 | 38.9±0.7 | 7.9±0.4 | 46.7±0.4 | 26.8±0.4 | 30.3 |

Table 3: Accuracy (%) on the DomainNet dataset (Peng et al., 2018) dataset under UFDA protocol. The upper table shows the results based on AlexNet (Krizhevsky et al., 2012) backbone and the table below are the results based on ResNet (He et al., 2016) backbone.

| Method | D,E,K → B | B,E,K → D | B,D,K → E | B,D,E → K | Average |
|-------------------------------|-----------------|-----------------|-----------------|-----------------|-------------|
| Source Only | 74.4±0.3 | 79.2±0.4 | 73.5±0.2 | 71.4±0.1 | 74.6 |
| <i>f</i> -DANN | 75.2±0.3 | 82.7±0.2 | 76.5±0.3 | 72.8±0.4 | 76.8 |
| AdaBN | 76.7±0.3 | 80.9±0.3 | 75.7±0.2 | 74.6±0.3 | 76.9 |
| AutoDIAL | 76.3±0.4 | 81.3±0.5 | 74.8±0.4 | 75.6±0.2 | 77.1 |
| <i>f</i> -DAN | 75.6±0.2 | 81.6±0.3 | 77.9±0.1 | 73.2±0.2 | 77.6 |
| FADA+attention (I) | 74.8±0.2 | 78.9±0.2 | 74.5±0.3 | 72.5±0.2 | 75.2 |
| FADA+adversarial (II) | 79.7±0.2 | 81.1±0.1 | 77.3±0.2 | 76.4±0.2 | 78.6 |
| FADA+disentangle (III) | 78.1±0.2 | 82.7±0.1 | 77.4±0.2 | 77.5±0.3 | 78.9 |

Table 4: Accuracy (%) on “Amazon Review” dataset with unsupervised federated domain adaptation protocol.

the pre-trained parameters as it will take more time for those parameters to converge. Details of our model are listed in Table 8 (supplementary material).

Results and Analysis The experimental results on Office-Caltech10 datasets are shown in Table 2. We utilize the same backbones as the baselines and separately show the results. We make the following observations from the results: (1) Our model achieves **86.5%** accuracy with an AlexNet backbone and **87.1%** accuracy with a ResNet backbone, outperforming the compared baselines. (2) All the models have similar performance when **C,D,W** are selected as the target domain, but perform worse when **A** is selected as the target domain. This phenomenon is probably caused by the large domain gap, as the images in **A** are collected from `amazon.com` and contain a white background.

To better analyze the effectiveness of FADA, we perform the following empirical analysis: (1) **\mathcal{A} -distance** Ben-David et al. (2010) suggests \mathcal{A} -distance as a measure of domain discrepancy. Following Long et al. (2015), we calculate the approximate \mathcal{A} -distance $\hat{d}_{\mathcal{A}} = 2(1 - 2\epsilon)$ for **C,D,W**→**A** and **A,C,W**→**D** tasks, where ϵ is the generalization error of a two-sample classifier (e.g. kernel SVM) trained on the binary problem of distinguishing input samples between the source and target domains. In Figure 4(a), we plot for tasks with raw ResNet features, *f*-DANN features, and FADA features, respectively. We observe that the $\hat{d}_{\mathcal{A}}$ on DADA features are smaller than ResNet features and *f*-DANN features, demonstrating that FADA features are harder to be distinguished between source and target. (2) To show how the dynamic attention mechanism benefits the training process, we plot the training loss *w/* or *w/o* dynamic weights for **A,C,W**→**D** task in Figure 4(b). The figure shows the target model’s training error is much smaller when dynamic attention is applied, which is consistent with the quantitative results. In addition, in **A,C,W**→**D** setting, the weight of **A** decreases to the lower bound after first a few epochs and the weight of **W** increases during the training process, as photos in both **D** and **W** are taken in the same environment with different cameras. (3) To better analyze the error mode, we plot the confusion matrices for *f*-DAN and FADA on **A,C,D**→**W** task in Figure 4(c)-4(d). The figures show that *f*-DAN mainly confuses “calculator” vs. “keyboard”, “backpack” with “headphones”, while FADA is able to distinguish them with disentangled features.

| target | <i>mm</i> | <i>mt</i> | <i>sv</i> | <i>sy</i> | <i>up</i> | Avg | A | C | D | W | Avg | B | D | E | K | Avg |
|----------------------------|-----------|-----------|-----------|-----------|-----------|-------------|----------|----------|----------|----------|-------------|----------|----------|----------|----------|-------------|
| FADA w/o. attention | 60.1 | 91.2 | 49.2 | 69.1 | 90.2 | 71.9 | 83.3 | 85.7 | 86.2 | 88.3 | 85.8 | 77.2 | 82.8 | 77.2 | 76.3 | 78.3 |
| FADA w. attention | 62.5 | 91.4 | 50.5 | 71.8 | 91.7 | 73.6 | 84.2 | 88.7 | 87.1 | 88.1 | 87.1 | 78.1 | 82.7 | 77.4 | 77.5 | 78.9 |

Table 5: The ablation study results show that the dynamic attention module is essential for our model.

5.3 EXPERIMENTS ON DOMAINNET

DomainNet² This dataset contains approximately 0.6 million images distributed among 345 categories. It comprises of six domains: *Clipart* (*clp*), a collection of clipart images; *Infograph* (*inf*), infographic images with specific object; *Painting* (*pnt*), artistic depictions of object in the form of paintings; *Quickdraw* (*qdr*), drawings from the worldwide players of game “Quick Draw!”³; *Real* (*rel*), photos and real world images; and *Sketch* (*skt*), sketches of specific objects. This dataset is very large-scale and contains rich and informative vision cues across different domains, providing a good testbed for unsupervised federated domain adaptation. Some sample images can be found in Figure 2.

Results The experimental results on DomainNet are shown in Table 3. Our model achieves **28.9%** and **30.3%** accuracy with AlexNet and ResNet backbone, respectively. In both scenarios, our model outperforms the baselines, demonstrating the effectiveness of our model on large-scale dataset. Note that this dataset contains about 0.6 million images, and so even a one-percent performance improvement is not trivial. From the experiment results, we can observe that all the models deliver less desirable performance when *infograph* and *quickdraw* are selected as the target domains. This phenomenon is mainly caused by the large domain shift between *inf/qdr* domain and other domains.

5.4 EXPERIMENTS ON AMAZON REVIEW

Amazon Review (Blitzer et al., 2007a) This dataset provides a testbed for cross-domain sentimental analysis of text. The task is to identify whether the sentiment of the reviews is positive or negative. The dataset contains reviews from `amazon.com` users for four popular merchandise categories: *Books* (**B**), *DVDs* (**D**), *Electronics* (**E**), and *Kitchen appliances* (**K**). Following Gong et al. (2013), we utilize 400-dimensional bag-of-words representation and leverage a fully connected deep neural network as the backbone. The detailed architecture of our model can be found in Table 7 (supplementary materials).

Results The experimental results on Amazon Review dataset are shown in Table 4. Our model achieves an accuracy of **78.9%** and outperforms the compared baselines. We make two major observations from the results: (1) Our model is not only effective on vision tasks but also performs well on linguistic tasks under UFDA learning schema. (2) From the results of model **I** and **II**, we can observe the dynamic attention and federated adversarial alignment are beneficial to improve the performance. However, the performance boost from Model **II** to Model **III** is limited. This phenomenon shows that the linguistic features are harder to disentangle comparing to visual features.

5.5 ABLATION STUDY

To demonstrate the effectiveness of dynamic attention, we perform the ablation study analysis. The Table 5 shows the results on “Digit-Five”, Office-Caltech10 and Amazon Review benchmark. We observe that the performance drops in most of the experiments when dynamic attention model is **not** applied. The dynamic attention model is devised to cope with *the varying convergence rates in the federated learning system*, i.e., different source domains have their own convergence rate. In addition, it will increase the weight of a specific domain when the domain shift between that domain and the target domain is small, and decrease the weight otherwise.

6 CONCLUSION

In this paper, we first proposed a novel unsupervised federated domain adaptation (UFDA) problem and derived a theoretical generalization bound for UFDA. Inspired by the theoretical results, we

²<http://ai.bu.edu/M3SDA/>

³<https://quickdraw.withgoogle.com/data>

proposed a novel model called Federated Adversarial Domain Adaptation (FADA) to transfer the knowledge learned from distributed source domains to an unlabeled target domain with a novel dynamic attention schema. Empirically, we showed that feature disentanglement boosts the performance of FADA in UFDA tasks. An extensive empirical evaluation on UFDA vision and linguistic benchmarks demonstrated the efficacy of FADA against several domain adaptation baselines.

REFERENCES

- Mohamed Ishmael Belghazi, Aristide Baratin, Sai Rajeshwar, Sherjil Ozair, Yoshua Bengio, Aaron Courville, and Devon Hjelm. Mutual information neural estimation. In Jennifer Dy and Andreas Krause (eds.), *Proceedings of the 35th International Conference on Machine Learning*, volume 80 of *Proceedings of Machine Learning Research*, pp. 531–540, Stockholmsmässan, Stockholm Sweden, 10–15 Jul 2018. PMLR. URL <http://proceedings.mlr.press/v80/belghazi18a.html>.
- Shai Ben-David, John Blitzer, Koby Crammer, Fernando Pereira, et al. Analysis of representations for domain adaptation. *Advances in neural information processing systems*, pp. 137–144, 2007.
- Shai Ben-David, John Blitzer, Koby Crammer, Alex Kulesza, Fernando Pereira, and Jennifer Wortman Vaughan. A theory of learning from different domains. *Machine learning*, 79(1-2):151–175, 2010.
- Yoshua Bengio, Aaron Courville, and Pascal Vincent. Representation learning: A review and new perspectives. *IEEE transactions on pattern analysis and machine intelligence*, 35(8):1798–1828, 2013.
- J. Blitzer, M. Dredze, and F. Pereira. Biographies, bollywood, boom-boxes and blenders: Domain adaptation for sentiment classification. *Proceedings of the 45th annual meeting of the association of computational linguistics*, pp. 440–447, 2007a.
- John Blitzer, Koby Crammer, Alex Kulesza, Fernando Pereira, and Jennifer Wortman. Learning bounds for domain adaptation. In *Proc. NIPS*, 2007b.
- John Blitzer, Koby Crammer, Alex Kulesza, Fernando Pereira, and Jennifer Wortman. Learning bounds for domain adaptation. In J. C. Platt, D. Koller, Y. Singer, and S. T. Roweis (eds.), *Advances in Neural Information Processing Systems 20*, pp. 129–136. Curran Associates, Inc., 2008. URL <http://papers.nips.cc/paper/3212-learning-bounds-for-domain-adaptation.pdf>.
- Keith Bonawitz, Vladimir Ivanov, Ben Kreuter, Antonio Marcedone, H Brendan McMahan, Sarvar Patel, Daniel Ramage, Aaron Segal, and Karn Seth. Practical secure aggregation for privacy-preserving machine learning. In *Proceedings of the 2017 ACM SIGSAC Conference on Computer and Communications Security*, pp. 1175–1191. ACM, 2017.
- Fabio Maria Carlucci, Lorenzo Porzi, Barbara Caputo, Elisa Ricci, and Samuel Rota Bulò. Autodial: Automatic domain alignment layers. In *International Conference on Computer Vision*, 2017.
- Jia Deng, Wei Dong, Richard Socher, Li-Jia Li, Kai Li, and Li Fei-Fei. Imagenet: A large-scale hierarchical image database. In *Computer Vision and Pattern Recognition, 2009. CVPR 2009. IEEE Conference on*, pp. 248–255. IEEE, 2009.
- Geoff French, Michal Mackiewicz, and Mark Fisher. Self-ensembling for visual domain adaptation. In *International Conference on Learning Representations*, 2018. URL <https://openreview.net/forum?id=rkpoTaxA->.
- Yaroslav Ganin and Victor Lempitsky. Unsupervised domain adaptation by backpropagation. In Francis Bach and David Blei (eds.), *Proceedings of the 32nd International Conference on Machine Learning*, volume 37 of *Proceedings of Machine Learning Research*, pp. 1180–1189, Lille, France, 07–09 Jul 2015. PMLR. URL <http://proceedings.mlr.press/v37/ganin15.html>.
- Muhammad Ghifary, W Bastiaan Kleijn, and Mengjie Zhang. Domain adaptive neural networks for object recognition. In *Pacific Rim international conference on artificial intelligence*, pp. 898–904. Springer, 2014.

- Muhammad Ghifary, W Bastiaan Kleijn, Mengjie Zhang, David Balduzzi, and Wen Li. Deep reconstruction-classification networks for unsupervised domain adaptation. In *European Conference on Computer Vision*, pp. 597–613. Springer, 2016.
- Ran Gilad-Bachrach, Nathan Dowlin, Kim Laine, Kristin Lauter, Michael Naehrig, and John Wernsing. Cryptonets: Applying neural networks to encrypted data with high throughput and accuracy. In *International Conference on Machine Learning*, pp. 201–210, 2016.
- Boqing Gong, Yuan Shi, Fei Sha, and Kristen Grauman. Geodesic flow kernel for unsupervised domain adaptation. In *Computer Vision and Pattern Recognition (CVPR), 2012 IEEE Conference on*, pp. 2066–2073. IEEE, 2012.
- Boqing Gong, Kristen Grauman, and Fei Sha. Connecting the dots with landmarks: Discriminatively learning domain-invariant features for unsupervised domain adaptation. In *International Conference on Machine Learning*, pp. 222–230, 2013.
- Ian Goodfellow, Jean Pouget-Abadie, Mehdi Mirza, Bing Xu, David Warde-Farley, Sherjil Ozair, Aaron Courville, and Yoshua Bengio. Generative adversarial nets. In *Advances in neural information processing systems*, pp. 2672–2680, 2014.
- Arthur Gretton, Karsten M Borgwardt, Malte Rasch, Bernhard Schölkopf, and Alex J Smola. A kernel method for the two-sample-problem. In *Advances in neural information processing systems*, pp. 513–520, 2007.
- Gregory Griffin, Alex Holub, and Pietro Perona. Caltech-256 object category dataset. 2007.
- Kaiming He, Xiangyu Zhang, Shaoqing Ren, and Jian Sun. Deep residual learning for image recognition. In *Proceedings of the IEEE conference on computer vision and pattern recognition*, pp. 770–778, 2016.
- Judy Hoffman, Eric Tzeng, Taesung Park, Jun-Yan Zhu, Phillip Isola, Kate Saenko, Alexei Efros, and Trevor Darrell. CyCADA: Cycle-consistent adversarial domain adaptation. In Jennifer Dy and Andreas Krause (eds.), *Proceedings of the 35th International Conference on Machine Learning*, volume 80 of *Proceedings of Machine Learning Research*, pp. 1989–1998, Stockholmsmässan, Stockholm Sweden, 10–15 Jul 2018. PMLR. URL <http://proceedings.mlr.press/v80/hoffman18a.html>.
- Sergey Ioffe and Christian Szegedy. Batch normalization: Accelerating deep network training by reducing internal covariate shift. In *International conference on machine learning*, pp. 448–456, 2015.
- Jack Kiefer, Jacob Wolfowitz, et al. Stochastic estimation of the maximum of a regression function. *The Annals of Mathematical Statistics*, 23(3):462–466, 1952.
- Taeksoo Kim, Moon-su Cha, Hyunsoo Kim, Jung Kwon Lee, and Jiwon Kim. Learning to discover cross-domain relations with generative adversarial networks. In Doina Precup and Yee Whye Teh (eds.), *Proceedings of the 34th International Conference on Machine Learning*, volume 70 of *Proceedings of Machine Learning Research*, pp. 1857–1865, International Convention Centre, Sydney, Australia, 06–11 Aug 2017. PMLR. URL <http://proceedings.mlr.press/v70/kim17a.html>.
- Diederik P Kingma and Max Welling. Auto-encoding variational bayes. *arXiv preprint arXiv:1312.6114*, 2013.
- Durk P Kingma, Shakir Mohamed, Danilo Jimenez Rezende, and Max Welling. Semi-supervised learning with deep generative models. In *Advances in neural information processing systems*, pp. 3581–3589, 2014.
- Alex Krizhevsky, Ilya Sutskever, and Geoffrey E Hinton. Imagenet classification with deep convolutional neural networks. In *Advances in neural information processing systems*, pp. 1097–1105, 2012.
- Yann LeCun, Léon Bottou, Yoshua Bengio, and Patrick Haffner. Gradient-based learning applied to document recognition. *Proceedings of the IEEE*, 86(11):2278–2324, 1998.

- Hsin-Ying Lee, Hung-Yu Tseng, Jia-Bin Huang, Maneesh Singh, and Ming-Hsuan Yang. Diverse image-to-image translation via disentangled representations. In Vittorio Ferrari, Martial Hebert, Cristian Sminchisescu, and Yair Weiss (eds.), *Computer Vision – ECCV 2018*, pp. 36–52, Cham, 2018. Springer International Publishing. ISBN 978-3-030-01246-5.
- Yanghao Li, Naiyan Wang, Jianping Shi, Jiaying Liu, and Xiaodi Hou. Revisiting batch normalization for practical domain adaptation. *arXiv preprint arXiv:1603.04779*, 2016.
- Alexander H. Liu, Yen-Cheng Liu, Yu-Ying Yeh, and Yu-Chiang Frank Wang. A unified feature disentangler for multi-domain image translation and manipulation. *CoRR*, abs/1809.01361, 2018a. URL <http://arxiv.org/abs/1809.01361>.
- Ming-Yu Liu and Oncel Tuzel. Coupled generative adversarial networks. In *Advances in neural information processing systems*, pp. 469–477, 2016.
- Yang Liu, Tianjian Chen, and Qiang Yang. Secure federated transfer learning. *arXiv preprint arXiv:1812.03337*, 2018b.
- Mingsheng Long, Yue Cao, Jianmin Wang, and Michael Jordan. Learning transferable features with deep adaptation networks. In Francis Bach and David Blei (eds.), *Proceedings of the 32nd International Conference on Machine Learning*, volume 37 of *Proceedings of Machine Learning Research*, pp. 97–105, Lille, France, 07–09 Jul 2015. PMLR. URL <http://proceedings.mlr.press/v37/long15.html>.
- Mingsheng Long, Han Zhu, Jianmin Wang, and Michael I. Jordan. Deep transfer learning with joint adaptation networks. In *Proceedings of the 34th International Conference on Machine Learning, ICML 2017, Sydney, NSW, Australia, 6-11 August 2017*, pp. 2208–2217, 2017. URL <http://proceedings.mlr.press/v70/long17a.html>.
- Mingsheng Long, Zhangjie Cao, Jianmin Wang, and Michael I Jordan. Conditional adversarial domain adaptation. In *Advances in Neural Information Processing Systems*, pp. 1640–1650, 2018.
- Alireza Makhzani, Jonathon Shlens, Navdeep Jaitly, Ian Goodfellow, and Brendan Frey. Adversarial autoencoders. *ICLR workshop*, 2016.
- Yishay Mansour, Mehryar Mohri, Afshin Rostamizadeh, and A R. Domain adaptation with multiple sources. In D. Koller, D. Schuurmans, Y. Bengio, and L. Bottou (eds.), *Advances in Neural Information Processing Systems 21*, pp. 1041–1048. Curran Associates, Inc., 2009.
- Michael F Mathieu, Junbo Jake Zhao, Junbo Zhao, Aditya Ramesh, Pablo Sprechmann, and Yann LeCun. Disentangling factors of variation in deep representation using adversarial training. In *Advances in Neural Information Processing Systems*, pp. 5040–5048, 2016.
- Payman Mohassel and Peter Rindal. Aby 3: a mixed protocol framework for machine learning. In *Proceedings of the 2018 ACM SIGSAC Conference on Computer and Communications Security*, pp. 35–52. ACM, 2018.
- Payman Mohassel and Yupeng Zhang. Secureml: A system for scalable privacy-preserving machine learning. In *2017 IEEE Symposium on Security and Privacy (SP)*, pp. 19–38. IEEE, 2017.
- Augustus Odena, Christopher Olah, and Jonathon Shlens. Conditional image synthesis with auxiliary classifier GANs. In Doina Precup and Yee Whye Teh (eds.), *Proceedings of the 34th International Conference on Machine Learning*, volume 70 of *Proceedings of Machine Learning Research*, pp. 2642–2651, International Convention Centre, Sydney, Australia, 06–11 Aug 2017. PMLR. URL <http://proceedings.mlr.press/v70/odena17a.html>.
- Sinno Jialin Pan and Qiang Yang. A survey on transfer learning. *IEEE Transactions on knowledge and data engineering*, 22(10):1345–1359, 2010.
- Xingchao Peng and Kate Saenko. Synthetic to real adaptation with generative correlation alignment networks. In *2018 IEEE Winter Conference on Applications of Computer Vision, WACV 2018, Lake Tahoe, NV, USA, March 12-15, 2018*, pp. 1982–1991, 2018. doi: 10.1109/WACV.2018.00219. URL <https://doi.org/10.1109/WACV.2018.00219>.

- Xingchao Peng, Qinxun Bai, Xide Xia, Zijun Huang, Kate Saenko, and Bo Wang. Moment matching for multi-source domain adaptation. *arXiv preprint arXiv:1812.01754*, 2018.
- Xingchao Peng, Zijun Huang, Ximeng Sun, and Kate Saenko. Domain agnostic learning with disentangled representations. In *ICML*, 2019.
- Joaquin Quionero-Candela, Masashi Sugiyama, Anton Schwaighofer, and Neil D. Lawrence. *Dataset Shift in Machine Learning*. The MIT Press, 2009. ISBN 0262170051, 9780262170055.
- Ronald L Rivest, Len Adleman, Michael L Dertouzos, et al. On data banks and privacy homomorphisms. *Foundations of secure computation*, 4(11):169–180, 1978.
- Kate Saenko, Brian Kulis, Mario Fritz, and Trevor Darrell. Adapting visual category models to new domains. In *European conference on computer vision*, pp. 213–226. Springer, 2010.
- Kuniaki Saito, Kohei Watanabe, Yoshitaka Ushiku, and Tatsuya Harada. Maximum classifier discrepancy for unsupervised domain adaptation. In *The IEEE Conference on Computer Vision and Pattern Recognition (CVPR)*, June 2018.
- Virginia Smith, Chao-Kai Chiang, Maziar Sanjabi, and Ameet S Talwalkar. Federated multi-task learning. In *Advances in Neural Information Processing Systems*, pp. 4424–4434, 2017.
- Baochen Sun and Kate Saenko. Deep CORAL: correlation alignment for deep domain adaptation. *CoRR*, abs/1607.01719, 2016. URL <http://arxiv.org/abs/1607.01719>.
- Robert Tibshirani, Guenther Walther, and Trevor Hastie. Estimating the number of clusters in a data set via the gap statistic. *Journal of the Royal Statistical Society: Series B (Statistical Methodology)*, 63(2):411–423, 2001.
- Eric Tzeng, Judy Hoffman, Ning Zhang, Kate Saenko, and Trevor Darrell. Deep domain confusion: Maximizing for domain invariance. *arXiv preprint arXiv:1412.3474*, 2014.
- Eric Tzeng, Judy Hoffman, Trevor Darrell, and Kate Saenko. Simultaneous deep transfer across domains and tasks. In *The IEEE International Conference on Computer Vision (ICCV)*, December 2015.
- Eric Tzeng, Judy Hoffman, Kate Saenko, and Trevor Darrell. Adversarial discriminative domain adaptation. In *Computer Vision and Pattern Recognition (CVPR)*, volume 1, pp. 4, 2017.
- V Vapnik and Vladimir Vapnik. *Statistical learning theory* wiley. *New York*, pp. 156–160, 1998.
- Zili Yi, Hao (Richard) Zhang, Ping Tan, and Minglun Gong. Dualgan: Unsupervised dual learning for image-to-image translation. In *ICCV*, pp. 2868–2876, 2017.
- Han Zhao, Shanghang Zhang, Guanhang Wu, José MF Moura, Joao P Costeira, and Geoffrey J Gordon. Adversarial multiple source domain adaptation. In *Advances in Neural Information Processing Systems*, pp. 8559–8570, 2018.
- Jun-Yan Zhu, Taesung Park, Phillip Isola, and Alexei A Efros. Unpaired image-to-image translation using cycle-consistent adversarial networks. In *Computer Vision (ICCV), 2017 IEEE International Conference on*, 2017.

7 MODEL ARCHITECTURE

We provide the detailed model architecture (Table 6 and Table 8) for each component in our model: Generator, Disentangler, Domain Classifier, Classifier and MINE.

| layer | configuration |
|------------------------------|---|
| Feature Generator | |
| 1 | Conv2D (3, 64, 5, 1, 2), BN, ReLU, MaxPool |
| 2 | Conv2D (64, 64, 5, 1, 2), BN, ReLU, MaxPool |
| 3 | Conv2D (64, 128, 5, 1, 2), BN, ReLU |
| Disentangler | |
| 1 | FC (8192, 3072), BN, ReLU |
| 2 | DropOut (0.5), FC (3072, 2048), BN, ReLU |
| Domain Identifier | |
| 1 | FC (2048, 256), LeakyReLU |
| 2 | FC (256, 2), LeakyReLU |
| Class Identifier | |
| 1 | FC (2048, 10), BN, Softmax |
| Reconstructor | |
| 1 | FC (4096, 8192) |
| Mutual Information Estimator | |
| fc1_x | FC (2048, 512), LeakyReLU |
| fc1_y | FC (2048, 512), LeakyReLU |
| 2 | FC (512,1) |

Table 6: Model architecture for digit recognition task (“Digit-Five” dataset). For each convolution layer, we list the input dimension, output dimension, kernel size, stride, and padding. For the fully-connected layer, we provide the input and output dimensions. For drop-out layers, we provide the probability of an element to be zeroed.

| layer | configuration |
|------------------------------|--------------------------------------|
| Feature Generator | |
| 1 | FC (400, 128), BN, ReLU |
| Disentangler | |
| 1 | FC (128, 64), BN, ReLU |
| 2 | DropOut (0.5), FC (64, 32), BN, ReLU |
| Domain Identifier | |
| 1 | FC (64, 32), LeakyReLU |
| 2 | FC (32, 2), LeakyReLU |
| Class Identifier | |
| 1 | FC (32, 2), BN, Softmax |
| Reconstructor | |
| 1 | FC (64, 128) |
| Mutual Information Estimator | |
| fc1_x | FC (32, 16), LeakyReLU |
| fc1_y | FC (32, 16), LeakyReLU |
| 2 | FC (16,1) |

Table 7: Model architecture for cross-doman sentimental analysis task (“Amazon Review” dataset (Blitzer et al., 2007a)). For the fully-connected layers (FC), we provide the input and output dimensions. For drop-out layers (Dropout), we provide the probability of an element to be zeroed.

| layer | configuration |
|---|---|
| Feature Generator: ResNet101 or AlexNet | |
| Disentangler | |
| 1 | Dropout(0.5), FC (2048, 2048), BN, ReLU |
| 2 | Dropout(0.5), FC (2048, 2048), BN, ReLU |
| Domain Identifier | |
| 1 | FC (2048, 256), LeakyReLU |
| 2 | FC (256, 2), LeakyReLU |
| Class Identifier | |
| 1 | FC (2048, 10), BN, Softmax |
| Reconstructor | |
| 1 | FC (4096, 2048) |
| Mutual Information Estimator | |
| fc1_x | FC (2048, 512), LeakyReLU |
| fc1_y | FC (2048, 512), LeakyReLU |
| 2 | FC (512,1) |

Table 8: Model architecture for image recognition task (Office-Caltech10 (Gong et al., 2012) and DomainNet (Peng et al., 2018)). For each convolution layer, we list the input dimension, output dimension, kernel size, stride, and padding. For the fully-connected layer, we provide the input and output dimensions. For drop-out layers, we provide the probability of an element to be zeroed.

8 DETAILS OF DATASETS

We provide the detailed information of datasets. For Digit-Five and DomainNet, we provide the train/test split for each domain. For Office-Caltech10, we provide the number of images in each domain. For Amazon review dataset, we show the detailed number of positive reviews and negative reviews for each merchandise category.

| Digit-Five | | | | | | | |
|------------------|---------------|----------------|--------------------|----------------|-------------|------------|---------|
| Splits | <i>mnist</i> | <i>mnist_m</i> | <i>svhn</i> | <i>syn</i> | <i>usps</i> | Total | |
| Train | 25,000 | 25,000 | 25,000 | 25,000 | 7,348 | 107,348 | |
| Test | 9,000 | 9,000 | 9,000 | 9,000 | 1,860 | 37,860 | |
| Office-Caltech10 | | | | | | | |
| Splits | <i>Amazon</i> | <i>Caltech</i> | <i>Dslr</i> | <i>Webcam</i> | Total | | |
| Total | 958 | 1,123 | 157 | 295 | 2,533 | | |
| DomainNet | | | | | | | |
| Splits | <i>clp</i> | <i>inf</i> | <i>pnt</i> | <i>qdr</i> | <i>rel</i> | <i>skt</i> | Total |
| Train | 34,019 | 37,087 | 52,867 | 120,750 | 122,563 | 49,115 | 416,401 |
| Test | 14,818 | 16,114 | 22,892 | 51,750 | 52,764 | 21,271 | 179,609 |
| Amazon Review | | | | | | | |
| Splits | <i>Books</i> | <i>DVDs</i> | <i>Electronics</i> | <i>Kitchen</i> | Total | | |
| Positive | 1,000 | 1,000 | 1,000 | 1,000 | 4,000 | | |
| Negative | 1,000 | 1,000 | 1,000 | 1,000 | 4,000 | | |

Table 9: Detailed number of samples we used in our experiments.

9 PROOF OF THEOREM 2

Theorem 3. (Weighted error bound for federated domain adaptation). Let \mathcal{H} be a hypothesis class with VC-dimension d and $\{\hat{\mathcal{D}}_{S_i}\}_{i=1}^N, \hat{\mathcal{D}}_T$ be empirical distributions induced by a sample of size m from each source domain and target domain in a federated learning system, respectively. Then, $\forall \alpha \in \mathbb{R}_+^N, \sum_{i=1}^N \alpha_i = 1$, with probability at least $1 - \delta$ over the choice of samples, for each $h \in \mathcal{H}$,

$$\epsilon_T(h_T) \leq \underbrace{\hat{\epsilon}_{\tilde{S}}(\sum_{i \in [N]} \alpha_i h_{S_i})}_{\text{error on source}} + \sum_{i \in [N]} \alpha_i \underbrace{\left(\frac{1}{2} \hat{d}_{\mathcal{H}\Delta\mathcal{H}}(\hat{\mathcal{D}}_{S_i}, \hat{\mathcal{D}}_T) + \lambda_i \right)}_{(\mathcal{D}_{S_i}, \mathcal{D}_T) \text{ divergence}} + 4 \underbrace{\sqrt{\frac{2d \log(2Nm) + \log(4/\delta)}{Nm}}}_{\text{VC-Dimension Constraint}} \quad (9)$$

where λ_i is the risk of the optimal hypothesis on the mixture of \mathcal{D}_{S_i} and T , and \tilde{S} is the mixture of source samples with size Nm .

Proof. Consider a combined source domain which is equivalent to a mixture distribution of the N source domains, with the mixture weight α , where $\alpha \in \mathbb{R}_+^N$ and $\sum_{i=1}^N \alpha_i = 1$. Denote the mixture source domain distribution as \tilde{D}_S^α (where $\tilde{D}_S^\alpha := \sum_{i \in [N]} \alpha_i \mathcal{D}_{S_i}$), and the data sampled from \tilde{D}_S^α as \tilde{S} . Theoretically, we can assume \tilde{D}_S^α and \mathcal{D}_T to be the source domain and target domain, respectively. Apply Theorem 1, we have that for $0 < \delta < 1$, with probability of at least $1 - \delta$ over the choice of samples, for each $h \in \mathcal{H}$,

$$\epsilon_T(h) \leq \hat{\epsilon}_{\tilde{S}}(h) + \frac{1}{2} \hat{d}_{\mathcal{H}\Delta\mathcal{H}}(\hat{\mathcal{D}}_{\tilde{S}}, \hat{\mathcal{D}}_T) + 4 \sqrt{\frac{2d \log(2Nm) + \log(4/\delta)}{Nm}} + \lambda_\alpha \quad (10)$$

where λ_α is the risk of optimal hypothesis on the \tilde{S} and T . The upper bound of $\hat{d}_{\mathcal{H}\Delta\mathcal{H}}(\hat{\mathcal{D}}_{\tilde{S}}, \hat{\mathcal{D}}_T)$ can be derived as follows:

$$\begin{aligned} \hat{d}_{\mathcal{H}\Delta\mathcal{H}}(\hat{\mathcal{D}}_{\tilde{S}}, \hat{\mathcal{D}}_T) &= 2 \sup_{A \in \mathcal{A}_{\mathcal{H}\Delta\mathcal{H}}} |\Pr(A) - \Pr(A)|_{\hat{\mathcal{D}}_{\tilde{S}} \hat{\mathcal{D}}_T} \\ &= 2 \sup_{A \in \mathcal{A}_{\mathcal{H}\Delta\mathcal{H}}} \left| \sum_{i \in [N]} \alpha_i \left(\Pr(A)_{\hat{\mathcal{D}}_{S_i}} - \Pr(A)_{\hat{\mathcal{D}}_T} \right) \right| \\ &\leq 2 \sup_{A \in \mathcal{A}_{\mathcal{H}\Delta\mathcal{H}}} \sum_{i \in [N]} \alpha_i \left(|\Pr(A)_{\hat{\mathcal{D}}_{S_i}} - \Pr(A)_{\hat{\mathcal{D}}_T}| \right) \\ &\leq 2 \sum_{i \in [N]} \alpha_i \sup_{A \in \mathcal{A}_{\mathcal{H}\Delta\mathcal{H}}} \left(|\Pr(A)_{\hat{\mathcal{D}}_{S_i}} - \Pr(A)_{\hat{\mathcal{D}}_T}| \right) \\ &= \sum_{i \in [N]} \alpha_i \hat{d}_{\mathcal{H}\Delta\mathcal{H}}(\hat{\mathcal{D}}_{S_i}, \hat{\mathcal{D}}_T) \end{aligned}$$

the first inequality is derived by the triangle inequality. Similarly, with the triangle inequality property, we can derive $\lambda_\alpha \leq \sum_{i \in [N]} \alpha_i \lambda_i$. On the other hand, for $\forall h_T \in \mathcal{H}$, we have: $\hat{\epsilon}_{\tilde{S}}(h_T) = \hat{\epsilon}_{\tilde{S}}(\sum_{i \in [N]} \alpha_i h_{S_i})$. Replace $\hat{\epsilon}_{\tilde{S}}(h)$, λ_α and $\hat{d}_{\mathcal{H}\Delta\mathcal{H}}(\hat{\mathcal{D}}_{\tilde{S}}, \hat{\mathcal{D}}_T)$ in Eq. 10, we have:

$$\begin{aligned} \epsilon_T(h_T) &\leq \hat{\epsilon}_{\tilde{S}}(h_T) + \frac{1}{2} \hat{d}_{\mathcal{H}\Delta\mathcal{H}}(\hat{\mathcal{D}}_{\tilde{S}}, \hat{\mathcal{D}}_T) + 4 \sqrt{\frac{2d \log(2Nm) + \log(4/\delta)}{Nm}} + \lambda_\alpha \\ &= \hat{\epsilon}_{\tilde{S}}(\sum_{i \in [N]} \alpha_i h_{S_i}) + \frac{1}{2} \hat{d}_{\mathcal{H}\Delta\mathcal{H}}(\hat{\mathcal{D}}_{\tilde{S}}, \hat{\mathcal{D}}_T) + 4 \sqrt{\frac{2d \log(2Nm) + \log(4/\delta)}{Nm}} + \lambda_\alpha \\ &\leq \hat{\epsilon}_{\tilde{S}}(\sum_{i \in [N]} \alpha_i h_{S_i}) + \frac{1}{2} \sum_{i \in [N]} \alpha_i \hat{d}_{\mathcal{H}\Delta\mathcal{H}}(\hat{\mathcal{D}}_{S_i}, \hat{\mathcal{D}}_T) + \sum_{i \in [N]} \alpha_i \lambda_i + 4 \sqrt{\frac{2d \log(2Nm) + \log(4/\delta)}{Nm}} \\ &= \underbrace{\hat{\epsilon}_{\tilde{S}}(\sum_{i \in [N]} \alpha_i h_{S_i})}_{\text{error on source}} + \sum_{i \in [N]} \alpha_i \underbrace{\left(\frac{1}{2} \hat{d}_{\mathcal{H}\Delta\mathcal{H}}(\hat{\mathcal{D}}_{S_i}, \hat{\mathcal{D}}_T) + \lambda_i \right)}_{(\mathcal{D}_{S_i}, \mathcal{D}_T) \text{ divergence}} + 4 \underbrace{\sqrt{\frac{2d \log(2Nm) + \log(4/\delta)}{Nm}}}_{\text{VC-Dimension Constraint}} \end{aligned}$$

□

Remark. The equation in Theorem 2 provides a theoretical error bound for unsupervised federated domain adaptation as it assumes that the source data distributed on different nodes can form a mixture source domain. In fact, the data on different node can not be shared under the federated learning schema. The theoretical error bound is only valid when the weights of models on all the nodes are fully synchronized.